Digest Journal of Nanomaterials and Biostructures Vol. 7, No. 3, July - September 2012, p. 1245 - 1252

EFFECTS OF TiC-PARTICULATE DISTRIBUTION IN AISI 304L STAINLESS STEEL MATRIX

A. P. I. POPOOLA[a*], B. A. OBADELE[a], O. M. POPOOLA[b]
[a]*Department of Chemical and Metallurgical Engineering, Tshwane University of Technology, P.M.B X680, Pretoria, South Africa, 0001.*
[b]*The Centre for Energy and Electric Power, Tshwane University of Technology, P.M.B. X680, Pretoria, South Africa, 0001.*

Homogeneous reinforcement particles distribution in the metal matrix is an important factor for obtaining high quality metal matrix composites (MMCs) with superior properties. Laser particle injection of AISI 304L austenitic stainless steel (ASS) was carried out with TiC as reinforcement powder. Characterization of MMCs fabricated was carried out using optical microscopy (OM), scanning electron microscopy (SEM) and X-ray diffraction (XRD) analyses. The effects of varying laser power and scan speed on the microstructure, hardness and corrosion properties evolved were investigated. Experimental results indicated that at scan speed of 0.6 m/min and laser power of 2.0 kW the MMC produced revealed a uniform distribution of TiC particulates in the modified zone, this sample also displayed significant increase in microhardness which is twice that of the AISI 304L stainless steel substrate. The injection of TiC particles to 304L ASS increased the presence of Ti/Cr rich carbides in the microstructure and this reduces the corrosion resistance. However, sample produced at a laser power 1.5 kW and scan speed 1.2 m/min, showed a positive shift in E_{corr}, and this was attributed to the lowest powder fraction of TiC in the MMC.

(Received May 16, 2012; Accepted August 29, 2012)

Keywords: Laser; Hardness; Microstructure; Corrosion

1. Introduction

Austenitic stainless steels have been widely used in industries owing to their excellent corrosion resistance, heat resistance and workability. However, the strength of austenitic stainless steels is relatively lower than that other alloyed steels, which restricts the further extension of their applications. This shortcoming is characteristic of the low surface hardness exhibited by this steel. However, AISI 304L stainless steels cannot be hardened through heat treatment due to its austenitic nature, in this respect laser surface modification technique can adequately fill this gap. Laser surface modification has been developed to be an all-important surface processing in many fields of applications. Several papers on laser particle injection have been reported in recent literature [1-4]. Laser particle injection of austenitic stainless steels is a widely used method for their surface properties modification. The rapid melting and solidification during laser melt injection produces fine grain microstructure as well as homogenization of reinforcement particles distribution. The rapid cooling is a key factor influencing microstructural changes and hence the enhancement of mechanical and chemical properties. This will inevitably extend the range of possible applications of the steel. It is evident that processing conditions affect the uniform distribution of TiC reinforcement in the melt pool [4]. These conditions include the laser power,

*Corresponding author: PopoolaAPI@tut.ac.za

scan speed and etc.

The incorporation of carbides using laser processing has been found to improve the wear and hardness of austenitic stainless steels. The surfaces produced differ from those produced by thermal spray techniques in that there is continuity in the chemical and mechanical properties at the coating-substrate interface [5].

In the present investigations, TiC particulate reinforced austenitic stainless steel has been fabricated using laser processing. Lately, the applications of carbides especially titanium carbide (TiC) composites have increased. This is as a result of the new and promising materials for wear-resistant parts and high temperature engineering structural components [6-8], high specific strength, low density and high elastic modulus [9-11]. TiC is a good reinforcement for metal matrix composites (MMCs) due to its high hardness, high melting point and relatively high thermal and chemical stabilities [12-15].

Laroudie et al. [16] studied the incorporation of C, TiC, SiC and ad-mixed Ti/SiC powders on 316L stainless steel. For TiC deposition, the laser coated surface appeared to be crack-free but non-uniformly distributed. Some large clusters of TiC which vary from 10 to 50 μm in size are distributed within the composite.

This work is aimed at investigating whether carbide formed AISI 304L MMCs could result in improved corrosion resistance. To obtain a high performance MMCs with controllable microstructures, TiC/AISI 304L matrix was prepared by laser processing under different processing parameters. The effect of laser power and scan speed on the microstructure and hardness were investigated.

2. Experimental details

AISI 304L austenitic stainless steel is the substrate material. The substrate was cut and machined to dimensions 80 x 60 x 6 mm. The surface of the substrate was sandblasted to improve absorption of the laser beam. X-ray diffractometer (XRD) was used to determine the phase composition of powder. The surface of the substrate was subjected to sandblasting, for the purposes of cleaning and improvement of the absorption of the laser beam.

A 4.4 kW Rofin Sinar continuous wave Nd: YAG laser was used to deliver the laser beam to the target surface. The reinforcing powder was fed into the melt pool by means of an argon gas stream. The shielding gas flow rate, powder feed rate and beam diameter were set at 2 L/min, 3 rpm and 3 mm respectively. Laser power was varied from 1.5-2.0 kW and scan speed was varied from 0.6-1.2 m/min.

Transverse sections of the laser deposited samples were cut for microstructural and micro-hardness analysis. The optical microscopy (OM) and scanning electron microscopy (SEM) equipped with energy dispersive spectrometry (EDS) were used for microstructural observation and microanalysis of composition. XRD was performed to identify the phases in the coatings.

Microhardness measurements were made using a Vickers Hardness Tester. Microhardness of samples were determined with 100 μm spacing between corresponding indentations using a load of 100 g for 10 s. An average of five indentations was taken as the micohardness of samples.

The corrosion behaviour of the specimen was studied in 3.5% NaCl solution using the linear potentiodynamic electrochemical measurement technique. All electrochemical measurements were carried out at room temperature (25 ± 1^{o}C) using an Autolab Potentiostat (PGSTAT20 computer controlled) general purpose electrochemical software (GPES) version 4.9. Potentiodynamic polarization curves were measured at a scan rate of 2 mV/s starting from -1.5 V (with respect to the OCP) to about 1.2 V. All the potentials reported were plotted versus the SCE potentials.

3. Result and discussions

3.1 Characterization of starting materials and fabricated MMCs

The nominal composition of 304L ASS used as the matrix is 18.7%Cr, 9.20%Cr, 0.45%Si, 1.5%Mn, 0.001%S, 0.027%P, 0.02%C and Fe balance. The carbon content of this steel is rather very low while the chromium content is high; hence this material has corrosion resistance.

The particle size of the TiC particles was found to be an average of 82 μm. It has been observed that the relative size of the particles influence the flow during laser particle injection, coarse particles tend to display smooth flow during injection. The purity of the powder was determined by EDS.

Single tracks were made on the sandblasted surfaces. The distribution states of the reinforcing particles in the MMCs manufactured under different processing parameters are shown in Fig. 1. The MMCs comprise partially or completely melted and reprecipitated TiC particulates. At a suitable laser power of 2.0 kW and scan speed of 0.6 m/min (sample 4) a sufficient amount of liquid phase was generated and this favours high deposition of the particles in the meltpool, thus a homogeneous distribution of the reinforcement in the matrix was achieved. According to Jiang and Kovacevic [4], the laser beam-scanning speeds likewise the varying power affect the distribution, size and morphology of the deposited beads. The faster the beam moves, the larger the dilution zone, and the smaller the build-up zone. In all the samples from Fig. 1(a)-(f) TiC agglomerates are observed at the upper part of the composite layer, however, no pores were formed. These agglomerates are due to the density difference between TiC and the substrate.

Laser power and scan speeds affect the sizes and morphologies of the deposited particulates. When the laser beam scans over the substrate, energy is directly absorbed from the laser by the solid particles through both bulk coupling and powder coupling mechanisms [17]. It could be seen from Fig. 1 that the laser melt zones are influenced severely by both power and speed. When the laser power was increased from 1.5 to 2 kW with the same scan speed of 0.6 m/min from Fig. 1(a) and 2(d), the volume of particulates deposited increased with uniform distribution in the meltpool. Also, the faster the speed of the beam, the smaller the volume and mass of the particulates deposited. The laser melt zone decreases as the scan speed increases as can be seen in Fig. 1(d) to 2(f). It is noted that the minimum scan speed, 0.6 m/min, leads to the largest laser melted zone and gives the best distribution of reinforcement, as shown in Fig. 1(d). This may result from the lower solidification rate that permitted good rearrangement of particles.

From Fig. 1(d) to 2(f), it can be seen that the interface morphologies between the laser coated zone and heat affected zone (HAZ) changed with the speed of the laser beam. By increasing the scan speeds, their curvatures decrease from a U-shape to V-shape. This is due to the variation in scan speed as this influence the melt pool formed. It has been reported that the curved interface (U-shape) has a better melting bond [14].

From these results, the sizes and morphologies of the laser coated zone are related to the laser power and scan speed. Laser power of 1.5 kW and scan speed of 1.0 and 1.2 m/min are not ideal for coating TiC/stainless steel matrix composites while a laser power of 2.0 kW and scan speed of 0.6 m/min is appropriate. The fine TiC precipitates would improve the overall mechanical properties of the composite.

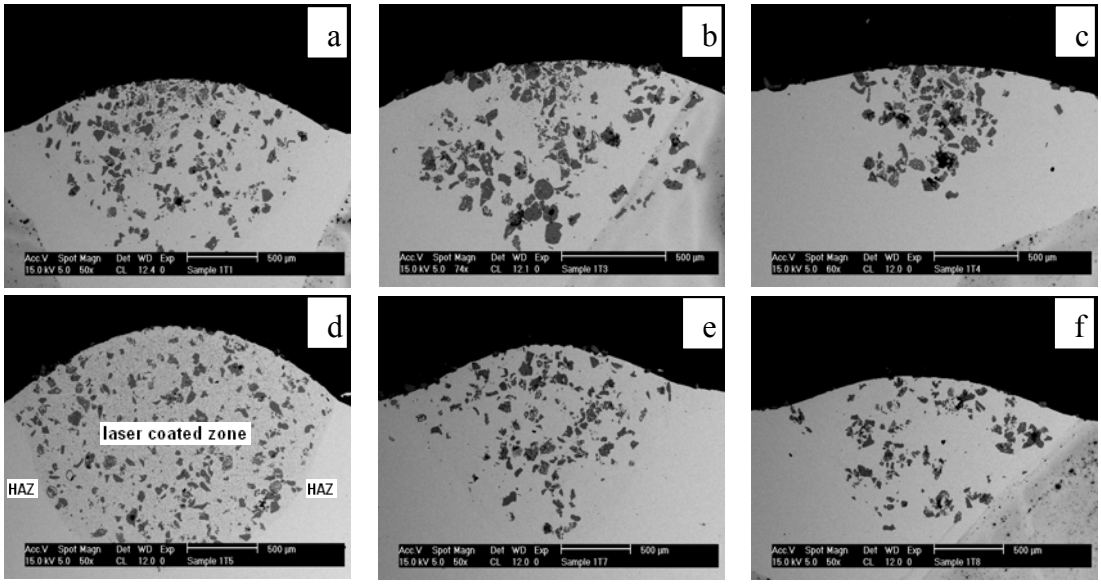

Fig. 1. Morphologies of TiC/stainless steel MMCs formed by single layer scanning at speeds and laser power of (a) 0.6 m/min, 1.5 kW; (b) 1.0 m/min, 1.5 kW; (c) 1.2 m/min, 1.5 kW; (d) 0.6 m/min, 2.0 kW; (e) 1.0 m/min, 2.0 kW and (f) 1.2 m/min, 2.0 kW.

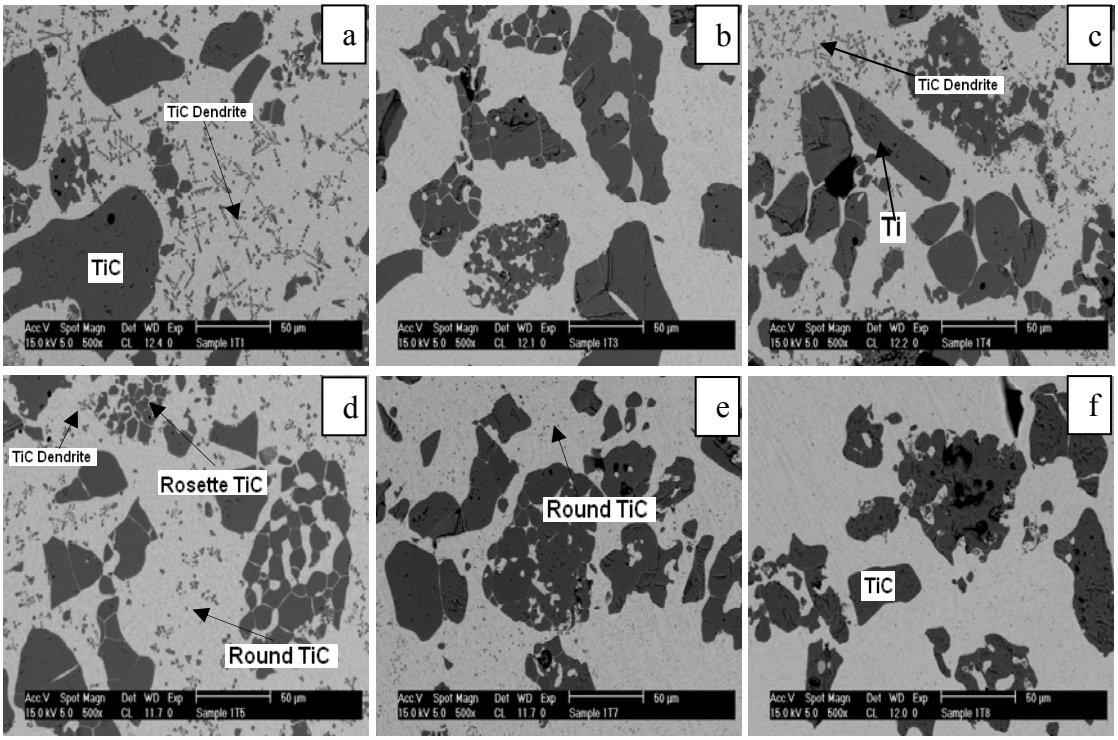

Fig. 2: SEM images of the TiC/stainless steel surface composite layers of Samples (a) 1, (b) 2, (c) 3, (d) 4, (e) 5 and (f) 6

Fig. 2(a)-(f) show high-magnification SEM micrographs of TiC particles in the composite layer. It indicates that TiC particles decompose and a great number of fine precipitates form during reactions and melt solidification. The precipitates appear fewer under low magnification in Fig. 1. TiC dendrite precipitates are found almost in all the coatings as indicated by the arrows. Round and faceted rosette-shaped primary TiC particles are found in sample 4.

EDS point analysis showed the presence of Ti, C and the matrix element, Fe. The XRD analysis results for specimen coated under laser power of 1.5 and 2.0 kW and scan speed 0.6

m/min are shown in Fig. 3. The analysis obtained indicated the formation of TiC on the steel surface. In all the specimens, high peaks of TiC and FeCrNi are observed. High peaks of TiC indicate a high volume fraction of the carbides in the matrix.

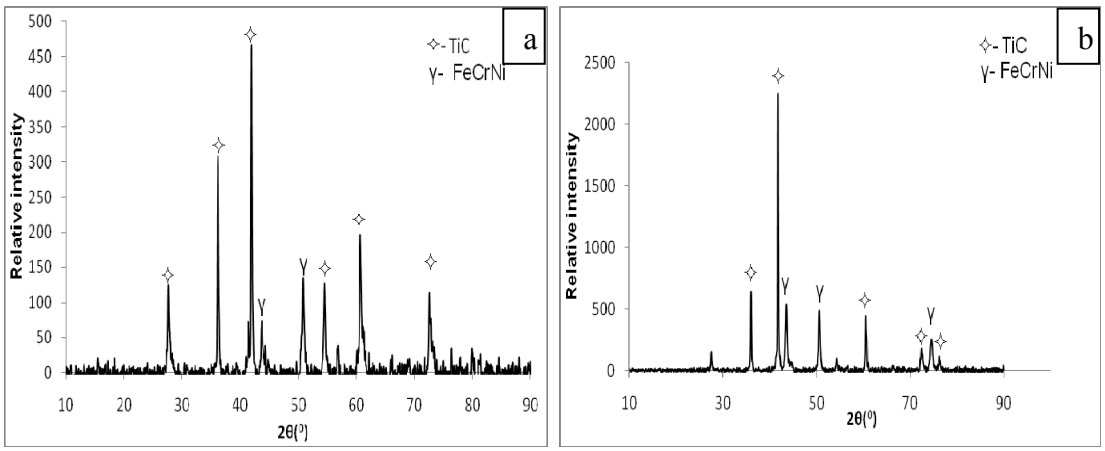

Fig. 3: X-ray diffraction results of specimen at scan speed of 0.6 m/min and laser power of (a) 1.5 and (b) 2.0 m/min.

Microhardness of the surface composite samples was measured along the depth from the irradiated surface. The results are shown in Fig. 4a. The average Vickers hardness of sample 1 is 406 $Hv_{0.1}$ and sample 4 is 443 $Hv_{0.1}$. The difference in microhardness value under the same scan speed of 0.6 m/min and different laser power of 1.5 and 2.0 kW could be as a result of the As it can be seen in Fig. 2 where more fine round TiC particulates are seen in sample 4 compared to TiC dendrites in sample 1. From Fig. 4b, sample D gave highest coating depth. This is due to the increase in laser power and a slower scan speed which leads to higher energy input and hence promoted a wider and deeper meltpool.

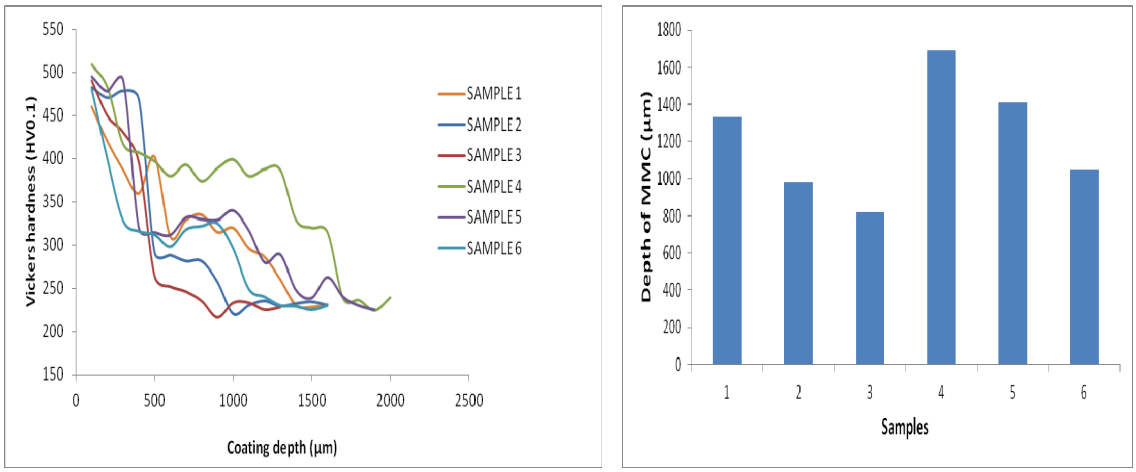

Fig. 4: Profiles for all MMCs (a) Hardness values and (a) Coating depth

Polarization curves for as-received and 304L/TiC samples in 3.5 wt.% NaCl solution under different processing parameters are shown in Fig. 5. Their E_{corr} and I_{corr} values are

summarized in Table 1. From Fig. 5, it can be deduced that the studied composites present an almost similar behavior in 3.5 wt% NaCl solution.

The as-received curve showed an active passive zone while the TiC/304L SS coatings showed a pseudo-passive zone. It revealed that the corrosion behavior of the laser treated samples was greatly influenced by the addition of TiC particle. The microstructure of treated samples resulted in discontinuous layer of Cr alloying elements in the matrix which led to decrease in corrosion resistance. The role of Cr is to form a passive layer on the surface of the alloy by forming Cr_2O_3 passive film [18] which is the primary reason for resistance to corrosion attained.

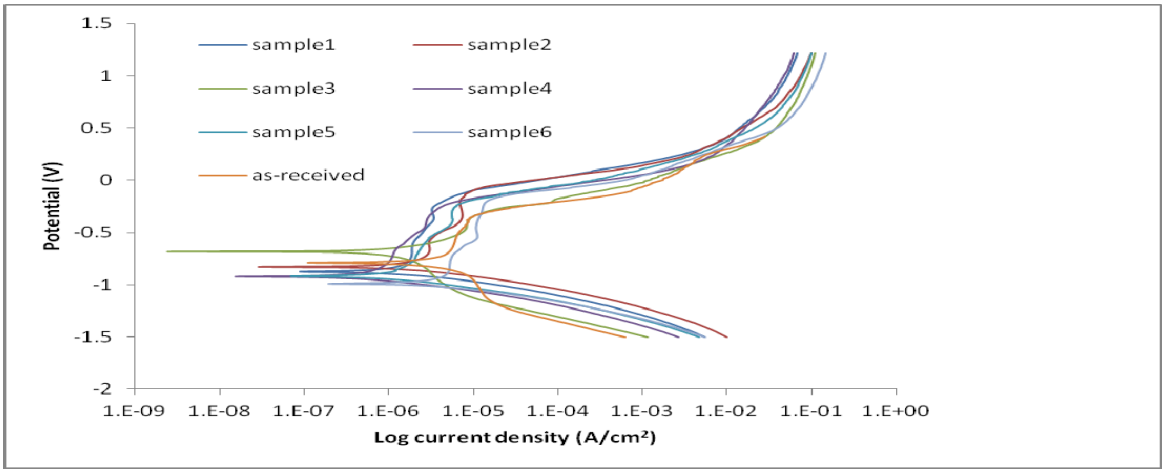

Fig. 5. Polarization curves of studied as-received and laser treated samples of 304L ASS exposed to 3.5% NaCl solution (potential scanning rate: 0.2 mV/S).

Comparing the 304L+TiC to as-received, Ecorr values had shifted to a more negative region along with increased Icorr values except for sample 3 which contain the least TiC particulates since it is processed at a low laser power of 1.5 kW and fastest scan speed of 1.2 m/min. This indicates that corrosion resistance decreases with more TiC in the matrix as shown in Table 1. The Ecorr value was more active for as-received, close to -0.79V than that for sample 3, which had a value of −0.68 V. Increased Ecorr values indicates resistance to corrosion. However, the corrosion current density value was higher for the as-received, $1.13x10^{-7}$ A/cm^2, than that for sample 3, 2.44×10^{-9} A/cm^2. A two order magnitude decrease in the current density was achieved meaning higher corrosion resistance for the fabricated MMC. Most techniques have shown that the addition of TiC particles decreased both the uniform corrosion rate of the base alloy and the resistance towards pitting type of corrosion [19]. Galvanic corrosion cell exist in the vicinity of TiC particles [18]. The presence of TiC could affect the quality of the passive film formed on the surface of the coatings. According to Wu et al [18], there is high probability that defects are introduced in the growing film due to the presence of matrix/TiC interfacial discontinuities. An increase in TiC content could further increase galvanic corrosion and the defects of the passive film.

Table 1: Electrochemical test parameters obtained from polarization curves.

Sample Labels	Medium	Specimen	E_{corr} (V_{sce})	I_{corr} (A/cm^2)	Laser power (kW)	Scan speed (m/min)
0	3.5% NaCl	304L	-0.79	1.13x10-7	-	-
1	3.5% NaCl	304L + TiC	-0.87	9.16x10-8	1.5	0.6
2	3.5% NaCl	304L + TiC	-0.83	2.93x10-8	1.5	1.0
3	3.5% NaCl	304L + TiC	-0.68	2.44 x 10-9	1.5	1.2
4	3.5% NaCl	304L + TiC	-0.92	1.53x10-8	2.0	0.6
5	3.5% NaCl	304L + TiC	-0.92	7.14x10-8	2.0	1.0
6	3.5% NaCl	304L + TiC	-0.99	7.07x10-7	2.0	1.2

4. Conclusions

Detailed investigations into the effects of processing parameters on the particulate dispersion in the TiC/stainless steel MMCs prepared by laser injection have been performed. The results can be summarized as follows:

The laser power and scan speed affect the size and morphology of the laser coated zone. For a given laser power of 2.0 kW and scan speed of 0.6 m/min the reinforced particulates gives a refined morphology and homogeneous particle dispersion due to sufficient liquid formation.

There is a significant increase in hardness for all the fabricated MMCs.

The addition of TiC particles to 304L ASS resulted in a shift of the Ecorr to more negative values, however, at a laser power of 1.5 kW and scan speed of 1.2 m/min, a more noble potential was achieved, the corrosion resistance achieved at this laser processing parameters can be attributed to very volume fraction of TiC in the matrix of the AISI304 stainless steel.

The addition of TiC and the high heat input from the laser promoted the formation of Cr-rich carbides which promoted the formation of a galvanic corrosion cell.

Acknowledgements

The authors thank the financial supports from the National Laser Centre and Tshwane University of Technology.

References

[1] M.J Hamedi, M.J Torkamany, J. Sabbaghzadeh, Opt. Laser Eng. **49**, 557−563 (2011).
[2] S.Z Shuja, B.S. Yilbas, Optics & Laser Technol. **43**, 765−775 (**2010**).
[3] D . Gu, Y. Shen, J. Xiao, Int. J. Ref. Met. Hard Mat. **26**, 411−422 (2008).
[4] W.H. Jiang, R. Kovacevic, J. Mat. Proc. Technol. **186**, 331−338 (2007).
[5] C. Tassin, F. Laroudie, M. Pons, L. Lelait, Surf. Coat. Technol. **76-77**, 450−455 (1995).
[6] J.C. Sánchez-López, D. Martínez-Martínez, M.D. Abad, A. Fernández, Surf. Coat. Technol. **204**, 947 (2009).
[7] O. Verezub, Z. Kálazi, G. Buza, N.V. Verezub, G. Kaptay, Surf. Coat Technol. **203**, 3049−3057 (2009).
[8] D. Vallauri, I.C. Atias Adrian, A. Chrysanthou, J. Euro. Cer. Soc. **28**, 1697−1713 (2008).
[9] H. Ding, X. Liu, L. Yu, G. Zhao, Scripta Materialia **57**, 575−578 (2007).
[10] D. Hill, R. Banerjee, D. Huber, J. Tiley, Scripta Materialia **52**, 387–392 (2005).
[11] W. Xiang, G. Peng-Tao, Transac. Nonfer. Met. Soc. China **17**, S546–S550 (2007).
[12] H.O. Pierson, Handbook of chemical vapour deposition. Noyes Publications, New Jersey, (1992).
[13] Y. Suda, H. Kawasaki, K. Doi, S. Hiraishi, Thin Sol. Films **374**, 282−286 (2000).

[14] Y. Wang, X. Zhang, F. Li, G. Zeng, Mat. Des. **20**, 233−236 (1999).
[15] Z.F. Ni, Y.S. Sun, F. Xue, J. Bai, Y.J. Lu Mat. Des. **32**, 1462−1467 (2011).
[16] F. Laroudie, C. Tassin, M. Pons, J. Physique IV **4**, C4−77−C−80 (1994).
[17] P. Fischer, V. Romano, H.P. Weber, N.P. Karapatis, E. Boillat, R. Glardon, Acta Materilia **51**, 1651−1652 (2003).
[18] Q. Wu, W. Li, N. Zhong, Corr. Sci. **53**, 4258–4264 (2011).
[19] L.A. Falcon, E.B. Bedolla, J. Lemus, C. Leon, I. Rosales, J.G. Gonzalez-Rodriguez, Int. J. Corr. **2011**, 1−7 (2011).